Precipitation and growth behavior of RuO2 crystals in simplified nuclear waste glass

SONG, Wenfeng, MENG, Xiangda, NIU, Chenchen, DENG, Wei <http://orcid.org/0000-0002-1793-8455>, ZHOU, Zizheng, MEI, Yahui, OJOVAN, Michael, XU, Kai <http://orcid.org/0000-0002-6847-1277> and ZHAO, Qingbin

Precipitation and growth behavior of RuO_2 crystals in simplified nuclear waste glass

Wenfeng Song[a], Xiangda Meng[b], Chenchen Niu[a], Wei Deng[a], Zizheng Zhou[b], Yahui Mei[b], Michael Ojovan[a], Kai Xu[a,*], Qingbin Zhao[b,**]

[a] *State Key Laboratory of Silicate Materials for Architectures, Wuhan University of Technology, Wuhan 430070, P.R. China*

[b] *China Nuclear Power Engineering Co., Ltd. (CNPE), Beijing, 100840, PR China*

[*] Corresponding author. E-mail: kaixu@whut.edu.cn

[**] Corresponding author. E-mail: zhaoqb@cnpe.cc

Abstract

Ruthenium (Ru), an important fission product in spent nuclear fuel, has low solubility in borosilicate glass and tends to precipitate during the vitrification process, which may adversely affect the stability and performance of the final waste form. In this work, the precipitation behavior of RuO_2 in a simplified borosilicate glass system was systematically studied. The results showed that at 1200 °C, the solubility of Ru was less than 200 ppm, and nanocrystalline RuO_2 began to form when the concentration exceeded this limit. About 80% of the excess Ru was retained in the glass in the form of crystals, whereas about 20% volatilized. RuO_2 initially precipitated as flower-like clusters and then transformed into granular particles through a diffusion-controlled growth process. When the melting time exceeded 50 min, the crystal growth was significantly enhanced because of surface energy-driven particle aggregation. This study offers valuable insights into the precipitation and growth mechanism of RuO_2 in borosilicate glass melts, which is crucial for optimizing the vitrification process and controlling noble metal behavior in nuclear waste immobilization.

Keywords: Nuclear waste; Vitrification; Precipitation; Growth; Granular RuO_2; Ostwald ripening

1. Introduction

The high chemical durability and excellent thermal stability of the borosilicate glass matrix make it a preferred matrix for the immobilization of high-level liquid waste (HLLW) [1, 2]. HLLW generated from the high burnup spent fuel reprocessing process contains high proportions of platinum group metals (PGMs), including ruthenium (Ru), rhodium (Rh), and palladium (Pd)[3–5], which have low solubility in borosilicate glass (<500 ppm)[6, 7] and can precipitate as metals or oxides[8–10]. These precipitated crystals easily settle at the bottom of the melt to form a thick sludge layer, which partially or completely blocks the riser[11–14], resulting in furnace outlet blockage and thus obstruction of the glass discharge from the melter[8, 15–18]. The PGMs content in HLLW is about 6.5 kg/tU, with Ru having the highest content and accounting for more than 50% of all PGMs[19–21]. Consequently, studying the precipitation and growth behavior of Ru in the vitrification process is imperative.

The morphological features of precipitated RuO_2 in simulated nuclear glass have been extensively investigated. For example, granular or acicular RuO_2 crystals and a rutile structure $(Ru,Rh)O_2$ solid solution usually agglomerate in a glass melt, which significantly increases the viscosity, density, and conductivity of the molten glass[3, 4, 9, 16, 22, 23]. Additionally, individual and clustered RuO_2 acts as a crystal nucleating agent to induce the formation of other crystal phases and spinel structures[24–26], but it does not compromise the leaching resistance of the nuclear waste glass[27–29]. Boucetta et al.[30] showed that the reaction between RuO_2 compounds and glass precursors during vitrification formed crystalline RuO_2 with granular or acicular morphologies. Usami et al.[14] found that when the dissolution rate of sodium in the glass matrix lags behind the reaction rate with RuO_2, sodium ruthenate is formed as an intermediate phase, which subsequently decomposes to generate needle-like RuO_2 crystals. Moreover, the formation of metallic ruthenium (Ru^0) during waste vitrification by controlling the reduction reaction was determined. For example, Laurin et al.[23] reported that undissolved RuO_2 particles are prone to redox reactions at high temperatures and that most RuO_2 particles and small amounts of Ru^0 particles precipitate in glass. Additionally, Ru^0 particles were found to form via a disproportionation reaction of

RuO_2 and an autocatalytic nucleation and growth mechanism involving the reduction of Ru^{4+} to Ru^0[23, 31]. At high temperatures (e.g., 1500 °C), many fine Ru^0 particles are formed, serving as nucleation sites that help capture volatile RuO_3 and RuO_4 and further support the growth of Ru^0 particles. Bell and Tagami[32] reported that RuO_2 reduction for $10^{-2} < p\ (O_2) < 1$ atm and RuO_2 decomposition ($RuO_2 \rightarrow Ru^0 + O_2 + \varepsilon$ (RuO_2 (g), RuO_3 (g), and RuO_4 (g)) occurred at 1542 and 1403 °C for $p(O_2)$ = 1 and 0.21 bar, respectively. However, to the best of the authors' knowledge, systematic studies on the precipitation and growth behavior of RuO_2 in glass are still lacking, despite its importance for evaluating the accumulation and settling of platinum group metals (PGMs) during high-level liquid waste (HLLW) vitrification.

In this work, a simplified nuclear waste glass system with various RuO_2 contents and melting processes was employed to study the precipitation and growth behavior of RuO_2 crystals during vitrification. The effect of the RuO_2 content, melting temperature, and holding time on crystal growth was investigated using inductively coupled plasma-mass spectrometry (ICP-MS), X-ray diffraction (XRD), and field emission scanning electron microscopy and energy spectroscopy (FESEM-EDS). Furthermore, the growth mechanism of granular RuO_2 crystals was elucidated to provide a scientific basis for assessing their evolution and deposition behavior in glass melts.

2. Materials and methods

2.1 Preparation of samples

A glass frit with a nominal composition of 50.00SiO_2-18.89B_2O_3-6.67Al_2O_3-13.33Na_2O-5.00CaO-2.78Li_2O-3.33ZrO_2 (wt.%) was prepared (Table 1). The raw materials used to prepare the batches were analytical-grade reagents, including SiO_2, B_2O_3, Al_2O_3, Na_2CO_3, $CaCO_3$, Li_2CO_3, and ZrO_2. First, 100 g of the batch was placed in a corundum crucible and melted in an electric furnace at 1200 °C for 1 h. Then, the melt was poured onto a copper plate, followed by air cooling and crushing to powder. Of the batch containing crushed base glass powder with different RuO_2 contents (0.01, 0.02, 0.04, 0.1, 0.5, 1.0, 4.0, and 6.0 wt.%), 3 g was then ground and mixed in an agate mortar for 15 min for homogeneity. The batch in a corundum crucible was subsequently melted at 1200 °C for 30 min under air, which resulted in glass samples containing

precipitated RuO_2. The vitrified samples containing 0.01, 0.02, 0.04, 0.1, 0.5, 1.0, 4.0, or 6.0 wt.% RuO_2 were labeled as Ru0.01, Ru0.02, Ru0.04, Ru0.1, Ru0.5, Ru1.0, Ru4.0, or Ru6.0, respectively, whereas the as-received pure RuO_2 and those heat-treated at 1200 °C for 30 min were labeled as PR and PR30, respectively. Additionally, the crushed base glass powder was mixed with 0.5 wt.% RuO_2, and 3 g of the sample was melted at 1000, 1100, 1200, 1300, and 1400 °C. After melting, the crucible was transferred to a muffle furnace for annealing at 400 °C for 2 h. During the entire experiment, the lid was firmly placed on the crucible to limit Ru component loss at elevated temperatures. The RuO_2–borosilicate glass composite samples were cut to thicknesses of 2–3 mm, followed by grinding and polishing to obtain flat faces.

2.2. Characterization of the samples

The sample was placed in a nickel crucible, followed by the addition of 0.5 g of Na_2CO_3, 0.5 g of $NaHCO_3$, and 1.5 g of NaOH. The mixture was then heated in a muffle furnace at 900 °C for 1 h. After cooling to room temperature, the residue was rinsed with dilute acid to remove any adhering material and transferred into a microwave digestion vessel. Subsequently, 8 mL of HCl:HNO_3 (3:1 in volume ratio) and 2 mL of HF were added to the vessel. The mixture was subjected to pre-digestion at 120 °C for 30 min, followed by complete microwave digestion. Finally, the digested solution was diluted to a total volume of 25 mL with deionized water. The Ru concentrations in the samples were measured using inductively coupled plasma-mass spectrometry (ICP-MS, PerkinElmer, NexION 300X). The Ru loss (L) was calculated using the following formula:

$$L = (1 - R) \times 100\% \quad (1)$$

$$R = \frac{C_T m_T}{C_0 m_0} \quad (2)$$

where m_0 and m_T represent the masses of the initial and heat-treated glass samples, respectively, and C_0 and C_T represent the Ru concentrations in the initial and heat-treated glass samples, respectively[2].

X-ray diffraction (XRD, Malvern Panalytical Empyrean) equipped with a 40 kV and 40 mA copper target radiation source was used to analyze the phase composition

of pure RuO_2 powder and RuO_2–borosilicate composite glass with a 2θ scanning range of 20–60° and a 0.02° step length. The diffraction patterns were refined using the Rietveld method in GSAS-II software to estimate the RuO_2 precipitation content. Additionally, 10 wt.% corundum (Al_2O_3) was used as the internal standard.

The Pt-sprayed glass composite samples were analyzed by scanning electron microscopy (FESEM, Zeiss Ultra Plus, X-Max 50 X-ray spectrometer) at an accelerating voltage of 5 keV. The SEM images were analyzed to calculate the crystal size via Image-Pro Plus 6.0 software.

3. Results

3.1 Effect of the RuO_2 content on precipitation

Microstructural images of glass samples with different RuO_2 contents (0.01, 0.02, 0.04, and 0.1 wt.%) are presented in Fig. 1. According to the SEM analysis, no visual crystalline phases were observed in the glass matrix with 0.01 wt.% RuO_2 (Fig. 1a). However, precipitated crystals began to emerge in the glass samples when the Ru content exceeded 0.01 wt.%. Notably, numerous dispersed flower-like clusters formed in the glass when the Ru content was 0.1 wt.% (the inset of Fig. 1d). Consequently, these observations indicated that the Ru solubility limit in this glass system was less than 200 ppm (equivalent to 0.02 wt.%), beyond which significant nucleation and growth occurred. In addition, the precipitated crystals were nonuniformly dispersed in the glass matrix (Fig. 1b, c and d), likely due to the large discrepancy in the densities of the glass and PGMs [20].

To identify the crystalline phase, the XRD patterns of glass samples with different RuO_2 contents subjected to heat treatment at 1200 °C for 30, 60, 120, and 180 min are presented in Fig. 2. The XRD patterns of the 0.5, 1.0, 4.0, and 6.0 wt.% RuO_2 glass samples presented three primary RuO_2 diffraction peaks at 2θ = 28.02°, 35.07°, and 54.27°, which corresponded to the (110), (101), and (211) diffraction planes, respectively. The RuO_2 diffraction peak gradually increased with increasing RuO_2 content, and more RuO_2 crystals precipitated in the glass. Additionally, the XRD pattern showed the diffraction peak of metallic Ru^0 at 2θ = 44.005°, which corresponded to the (101) diffraction plane. This phenomenon was consistent with the results reported by Okamoto et al.[23, 33]. However, the XRD pattern showed only one diffraction peak

corresponding to metallic Ru^0, indicating that the crystals that precipitated from the glass were primarily RuO_2. As shown in Fig. 3, scanning electron microscopy-energy dispersive X-ray spectroscopy (FESEM–EDS) was used to accurately identify the morphologies of RuO_2 and metallic Ru^0 in the Ru4.0 samples. Numerous granular crystals were dispersed in the glass matrix. The compositional analysis of the precipitated crystals on the basis of back-scattered SEM images with energy dispersive X-ray spectroscopy (EDS) indicated that the gray polyhedral crystals (spot A) and bright crystals (spot B) were primarily RuO_2 and metallic Ru^0, respectively.

Furthermore, the contents of the RuO_2 crystal and metallic Ru^0 precipitated from the glass were evaluated. As shown in Fig. 4a, the quantity of the precipitated RuO_2 crystalline phases increased from about 0.3 wt.% to 4.5 wt.% with increasing added RuO_2 content (0.5–6.0 wt.%), but the metallic Ru^0 content essentially remained constant. The quantitative analysis based on Rietveld-refined XRD patterns indicated that the overall Ru precipitation percentage reached about 80% (Fig. 4b). The crystallographic refined data of precipitated RuO_2 and Ru^0 from glass samples (in the Supplementary Information) confirmed the reliability of the results. Furthermore, this was corroborated by the Ru analysis with ICP-MS measurements, which suggested about 20% Ru volatilization, confirming the consistency and validity of the analytical results (Fig. 4b).

To elucidate the precipitation and growth evolution process of RuO_2 within the glass melt, the morphology and diameter size of both pure RuO_2 and heat-treated pure RuO_2 were observed and characterized. As illustrated in the corresponding morphologies of the PR and PR30 samples in Figs. 5a and b, they had predominantly rectangular nanorod and aggregated block-like particle shapes, and heat treatment at 1200 °C for 30 min significantly increased their diameter to hundreds of nanometers (Figs. 5d and e). The morphology and diameter size distribution of the precipitated RuO_2 crystals in the glass are shown in Fig. 5c, g, h and i. The results revealed that numerous flower-like clusters precipitated when the RuO_2 content was 0.5 wt.% (Fig. 5c), with crystal sizes ranging from 100 to 150 nm (Fig. 5f). The different morphologies of RuO_2 in samples PR30 and Ru0.5 indicate that RuO_2 may react with the glass melt

and subsequently reprecipitate. The morphology of the RuO_2 precipitates changed from flower-like clusters to granular clusters when the RuO_2 content > 0.5 wt.% (Figs. 5g-i). When the RuO_2 content was 1.0 wt.%, the sizes of the precipitated crystals were primarily distributed in the 300–350 nm and 400–450 nm ranges (Fig. 5j). When the RuO_2 content was >1.0 wt.%, the crystal sizes were primarily in the ranges of 350–400 nm and 450–600 nm (Figs. 5k and l). These results indicated that a higher RuO_2 content enhanced the agglomeration of the RuO_2 crystals in the glass, which improved the probability of mutual aggregation between the particles and promoted the growth of the RuO_2 crystals.

3.2 Effects of heat treatment temperature and duration on the growth of RuO_2

Although flower-like RuO_2 clusters were observed in our glass (Fig. 1d and Fig. 5c), their evolution process is not fully understood. To study the evolution and growth process of RuO_2 in glass as a function of heat treatment temperature and duration, the Ru0.5 sample was subjected to extensive analysis. SEM images of the Ru0.5 glass samples melted at various temperatures (1000, 1100, 1200, 1300, and 1400 °C) and durations (30, 60, and 120 min) are presented in Fig. 6. Large tracts of fine RuO_2 particles, which are much smaller than those with added RuO_2 particles, were dispersed in the glass matrix at 1000 °C, suggesting that their dissolution reactions with the glass melt at this stage (e.g., Region 1). When the temperature increased to 1100 °C for a short duration (~30 min), RuO_2 had the same morphology as that observed at 1000 °C but with a slightly increased particle size, and some white rod-like precipitates were present for a longer duration (e.g., Region 2). These findings indicated that RuO_2 began to precipitate from the glass melt. Numerous independent flower-like RuO_2 clusters appeared within the glass matrix after heat treatment for 30 min at 1200 °C. With further increases in temperature and duration, the RuO_2 crystals developed well-defined granular shapes (e.g., Region 3), suggesting that RuO_2 precipitation and further agglomerated growth from the glass melt initiated at 1200 °C. A three-dimensional (3-D) diagram was plotted to correlate the heat-treatment temperatures, durations, and average crystal sizes, which provided a model to predict the average sizes of the RuO_2 crystals precipitated from the waste glass heat-treated for different durations at 1200–

1400 °C (Fig. 7).

The morphology and size distribution of RuO_2 crystals in Ru0.5 glass at 1200 °C for 5, 50, 180, and 300 min are shown in Figs. 8a-h. When t = 5 min, the crystal sizes were concentrated in the 100–150 nm range (Fig. 8e). When t = 50 min, the crystals grow noticeably larger and begin to agglomerate, with the morphology evolving from nanoscale particles to granular shapes (Fig. 8b). Correspondingly, the size distribution shifts markedly toward the 400–500 nm range (Fig. 8f). This trend becomes even more pronounced after 180 min and 300 min of heat treatment, with the particle size distribution curve continuously shifting toward larger sizes (Figs. 8c, d, g and 8 h). The morphology and size distribution of RuO_2 crystals in the Ru0.5 glass at 1300 °C for 5, 50, 180, and 300 min are also shown in Figs. 8i-p. The increase in temperature and duration significantly promoted the growth of the RuO_2 crystals, which progressively coarsened. The particle size distributions in Fig. 8 reveal a gradual decrease in the population of fine crystals and an increase in larger ones over time, indicating a coarsening trend. This behavior, together with the linear correlation between r^3 and time shown in Fig. 9, supports the occurrence of Ostwald ripening driven by dissolution and reprecipitation. These observations suggest that with longer heat treatment durations, RuO_2 crystals grow through agglomeration and Ostwald ripening, resulting in a broadened size distribution that gradually shifts toward larger particle sizes.

4. Discussion

Previous studies reported that the solubility of Ru in glasses was determined by the glass composition, melting temperature, and oxygen partial pressure [6, 7, 34]. For example, the solubility of Ru in soda-silica glass can increase from 100 to 2000 ppm when the amount of alkali oxides and the melting temperature increase[35]. Additionally, the increased oxygen partial pressure from 1.0 to 8.4 atm at 1873 K in molten slag could also enhance Ru solubility from 100 to 500 ppm[6], likely owing to the stable Ru oxyanions with high-valence integrated with the glass network. The Ru solubility (<200 ppm) estimated in this work is comparable with that reported in previous studies [5, 35], indicating the reliability of our experiments. However, the present work concentrated on the precipitation and growth behavior of RuO_2 crystals in the glass matrix. Thus, the

following focuses on how heat-treatment conditions affect the nucleation, morphology, and diameter size distribution of precipitated RuO_2 phases. The predominant phase formed in the glass melt was RuO_2, accompanied by a small Ru^0 fraction. No other crystalline phases were detected throughout the melting process. The type of crystalline phase remained unchanged regardless of the initial RuO_2 content or the increase in the melting temperature and duration, which indicated stable crystallization behavior under the investigated conditions. The 20% volatilization of Ru did not significantly affect the content of the formed metallic Ru^0, which suggested that the redox equilibrium between Ru^{4+} and Ru^0 was established relatively early in the process and was not significantly influenced by prolonged heat treatment.

Compared with the initial state, the RuO_2 crystals in the glass melt exhibited significant morphological evolution, suggesting that a dissolution-reprecipitation mechanism occurred during vitrification. Specifically, it was presumed that the initially formed fine RuO_2 particles partially dissolved and reprecipitated to form larger and more well-defined crystals over time. This phenomenon was consistent with the Ostwald ripening mechanism, which describes the growth kinetics of particles in supersaturated solutions that have completed the nucleation stage [36, 37]. In essence, driven by a certain temperature, the high interface energy in an uneven particle system can reduce the system interface, leading to the migration of component solutes from small to large particles, the dissolution and disappearance of small particles, and the coarsening of large particles[38–40]. According to the basic principles of thermodynamics and the diffusion control mechanism, the relationship between the average crystal size of RuO_2 and the coarsening rate of crystal particles can be obtained and is given in Eq. (3).

$$r^3 - r_0^3 = Kt \quad (3)$$

where r, r_0, and K represent the average radius at any time (except t = 0), the average radius at t = 0, and the rate constant, respectively[10].

The time evolution of r^3 obtained from the average sizes measured at 1200 and 1300 °C is illustrated in Fig. 9. The linear fitting result implies that two different driving forces control growth, with each being dominant within a different time regime. In the

early stage of melting ($t \leq 50$ min), the RuO_2 growth behavior followed a diffusion-controlled mechanism. During this stage, particle diffusion played a critical role in controlling the kinetics of crystal growth since the RuO_2 particles reprecipitated and subsequently agglomerated in the glass melt. Notably, the curve corresponding to 1300 °C was significantly above that corresponding to 1200 °C, suggesting that elevated temperatures significantly promoted RuO_2 crystal growth and accelerated the reaction kinetics. However, the growth rate notably changed as the melting time increased beyond 50 min. This could be attributed to the increased particle size, which improved the probability of mutual aggregation of the particles. This particle-particle interaction introduced an additional driving force for crystal growth, which potentially shifted the mechanism to being interface controlled. Furthermore, these findings were supported by the microstructural observations presented in Fig. 8.

The formation process and evolution mechanism of granular RuO_2 crystals can be summarized as follows (Fig. 10). In the initial stage, RuO_2 particles reacted with the glass melt, and a small number of RuO_2 crystals were locally saturated and precipitated. As the melting duration increased, RuO_2 crystals further diffused into the melt and aggregated to form flower-like clusters (1200 °C, 30 min). With further extension of the melting duration (>30 min), RuO_2 crystals grew rapidly to form granular RuO_2 crystals due to the mutual aggregation of the particles; this process primarily depended on the Oswald ripening mechanism.

Interestingly, the RuO_2 crystals precipitated in this study exhibited only flower-like and granular morphologies, but acicular morphologies were not observed. The flower-like crystals appeared in the early stage of the precipitated RuO_2 crystal and transformed into granular shapes via Ostwald ripening upon further growth. Previous studies have suggested that the precipitation of needle-shaped RuO_2 crystals in glass is likely due to the formation of the intermediate phase of sodium ruthenate, which arises from the reaction between $NaNO_3$ and RuO_2[21]. In our study, the prepared base glass powder melted with pure RuO_2, and sodium ruthenate did not appear throughout the whole process, which might have caused only granular RuO_2 formation in the final stage of RuO_2 growth.

Although in the realistic HLLW vitrification process, other PGMs (Rh and Pd) as well as other components affect the crystalline phase, morphology, and growth of the precipitated PGMs, the study of the growth behavior of RuO_2 crystals in glass provides a scientific basis and supportive clue to fully understand the precipitation and growth of PGM-related phases during HLLW vitrification. More specifically, if the size of precipitated PGM-related phases is easily estimated through a kinetic model of PGM growth in a glass melt and the crucial factors controlling the growth of PGMs are determined, countermeasures could be applied to address the challenges associated with PGM-induced operation issues.

5. Conclusions

This study investigated the precipitation and growth behavior of RuO_2 working with simplified nuclear waste glass. The conclusions drawn were as follows:

(1) The solubility of Ru in borosilicate glass was less than 200 ppm, and initial nanocrystalline precipitates appeared for ≥ 0.02 wt.% RuO_2. The primary precipitation phase in the glass melt was RuO_2 crystals accompanied by small amounts of metallic Ru^0. The changes in the glass melting temperature, duration, and RuO_2 content did not significantly affect the crystal phase. The size of the RuO_2 crystals increased with increasing RuO_2 content, temperature, and duration. Furthermore, a higher RuO_2 content accelerated the agglomerated growth of the RuO_2 crystals.

(2) When T < 1200 °C, RuO_2 primarily underwent a reaction with the glass melt. At T ≥ 1200 °C, RuO_2 crystals begin to precipitate and further diffuse and agglomerate from the glass melt. The morphology of the RuO_2 crystals changed from initial nanoparticles to flower-like clusters and then agglomerated into granules.

(3) The growth rate constant of the RuO_2 crystals increased with increasing melting temperature and duration. The growth kinetics revealed that diffusion-controlled and surface energy-controlled mechanisms, following Oswald ripening, governed the growth-driving force of RuO_2 crystals.

Acknowledgments

The authors gratefully appreciate the financial support from the National Natural Science Foundation of China (No. U2241290).

Reference

[1] M.I. Ojovan, W.E. Lee, S.N. Kalmykov, An introduction to nuclear waste immobilisation, Elsevier, 2019.

[2] Z. Jia, C. Liu, C. Niu, K. Li, K. Xu, Volatilization of sodium and boron from nuclear waste glass and associated effects on glass structure and thermal stability, Journal of Nuclear Materials, 587 (2023) 154712.

[3] T. Sugawara, T. Ohira, S. Komamine, E. Ochi, Partitioning of rhodium and ruthenium between Pd–Rh–Ru and (Ru, Rh)O_2 solid solutions in high-level radioactive waste glass, Journal of Nuclear Materials, 465 (2015) 590-596.

[4] T. Hartmann, H. Pentinghaus, The ternary system palladium–rhodium–tellurium: A Study to understand phase formation in the vitrification process of high-level waste concentrates (HLWC), Journal of Nclear Materials, 422 (2012) 124-130.

[5] M. Yamashita, H. Yamanaka, K.i. Sasage, Dissolution and separation of ruthenium in borosilicate glass, Journal of the American Ceramic Society, 87 (2004) 967-969.

[6] H. Shuto, T.H. Okabe, K. Morita, Ruthenium solubility and dissolution behavior in molten slag, Materials Transactions, 52 (2011) 1899-1904.

[7] P. Palanisamy, D.H. Sarma, R.W. Vest, Solubility of ruthenium dioxide in lead borosilicate glasses, Journal of the American Ceramic Society, 72 (1989) 1755-1756.

[8] A. Borisov, L. Danyushevsky, The effect of silica contents on Pd, Pt and Rh solubilities in silicate melts: an experimental study, European Journal of Mineralogy, 23 (2011) 355-367.

[9] H. Kamat, B.I. Arias-Serrano, A. Yaremchenko, A. Goel, Ruthenium solubility and its impact on the crystallization behavior and electrical conductivity of MoO_3-containing borosilicate-based model high-level nuclear waste glasses, Journal of Non-Crystalline Solids, 549 (2020) 120356.

[10] R. Pflieger, L. Lefebvre, M. Malki, M. Allix, A. Grandjean, Behaviour of ruthenium dioxide particles in borosilicate glasses and melts, Journal of Nuclear Materials, 389 (2009) 450-457.

[11] J. Matyáš, J.D. Vienna, A. Kimura, M. Schaible, R.M. Tate, Development of crystal-tolerant waste glasses, Advances in Materials Science for Environmental and

Nuclear Technology, 222 (2010) 41-50.

[12] J. Matyas, A.R. Huckleberry, C.P. Rodriguez, J.B. Lang, A.T. Owen, A.A. Kruger, HLW glass studies: development of crystal-tolerant HLW glasses, in, Pacific Northwest National Lab.(PNNL), Richland, WA (United States), 2012.

[13] J. Matyáš, V. Gervasio, S.E. Sannoh, A.A. Kruger, Predictive modeling of crystal accumulation in high-level waste glass melters processing radioactive waste, Journal of Nuclear Materials, 495 (2017) 322-331.

[14] T. Usami, K. Uruga, T. Tsukada, Basic study of formation of acicular crystals by chemical reactions between RuO_2 and $NaNO_3$ in a waste vitrification process, Journal of Nuclear Science and Technology, 58 (2021) 751-763.

[15] R.B. Nuernberg, N.M.P. Machado, M. Malki, M. Neyret, Electrical behavior of RuO_2-glass composites: The effect of RuO_2 particle size on the percolation threshold, Journal of Nuclear Materials, 546 (2021) 152777.

[16] C. Hanotin, J. Puig, M. Neyret, P. Marchal, Platinum group metal particles aggregation in nuclear glass melts under the effect of temperature, Journal of Nuclear Materials, 477 (2016) 102-109.

[17] R.B. Nuernberg, N.M.P. Machado, D. Jouglard, L. del Campo, M. Malki, M. Neyret, The origin of hysteresis in the electrical behavior of RuO_2-glass composite melts, Journal of Non-Crystalline Solids, 557 (2021) 120596.

[18] K.S. Matlack, H. Gan, I.L. Pegg, I. Joseph, B.W. Bowan, Y. Miura, N. Kanehira, E. Ochi, T. Ebisawa, A. Yamazaki, Scaled melter testing of noble metals behavior with Japanese HLW streams, Ceramics for Environmental and Energy Applications II: Ceramic Transactions, Volume 246, (2014) 225-235.

[19] T. Ogawa, Percolation in Radioactive-Waste Glass Melt with RuO_2, Journal of the American Ceramic Society, 93 (2010) 2487-2490.

[20] R. Jia, C. Niu, X. Liu, M. Ojovan, L. Pereira, F.B. Wadsworth, K. Xu, A. Chen, Crystal spatial distribution controls the electrical response of nuclear waste glasses containing RuO_2 crystals, Journal of the American Ceramic Society, (2025) e20567.

[21] X. Duan, X. Liu, Z. Qian, Q. Zhang, L. Li, K. Zhang, Y. Qiao, Controlled growth of ruthenium dioxide nanostructures in borosilicate glass melts, Journal of Nuclear

Materials, 603 (2025) 155436.

[22] P.B. Rose, D.I. Woodward, M.I. Ojovan, N.C. Hyatt, W.E. Lee, Crystallisation of a simulated borosilicate high-level waste glass produced on a full-scale vitrification line, Journal of Non-Crystalline Solids, 357 (2011) 2989-3001.

[23] C. Laurin, E. Regnier, S. Gossé, A. Laplace, J. Agullo, S. Mure, E. Brackx, M. Toplis, O. Pinet, Redox behavior of ruthenium in nuclear glass melt: ruthenium dioxide reduction reaction, Journal of Nuclear Materials, 545 (2021) 152650.

[24] H. Mitamura, T. Murakami, T. Banba, Crystalline phases in a devitrified simulated high-level waste glass containing the elements of the platinum group, Journal of Nuclear Materials, 136 (1985) 104-116.

[25] C. Jantzen, D.F. Bickford, D.G. Karraker, Time-temperature-transformation kinetics in SRL waste glass, in, Du Pont de Nemours (EI) and Co., Aiken, SC (USA). Savannah River Lab., 1983.

[26] N. Chouard, D. Caurant, O. Majérus, J. Dussossoy, S. Klimin, D. Pytalev, R. Baddour-Hadjean, J. Pereira-Ramos, Effect of MoO_3, Nd_2O_3, and RuO_2 on the crystallization of soda–lime aluminoborosilicate glasses, Journal of Materials Science, 50 (2015) 219-241.

[27] M.I. Ojovan, V.A. Petrov, S.V. Yudintsev, Glass crystalline materials as advanced nuclear wasteforms, Sustainability, 13 (2021) 4117.

[28] C. Jantzen, M. Ojovan, On selection of matrix (wasteform) material for higher activity nuclear waste immobilization, Russian Journal of Inorganic Chemistry, 64 (2019) 1611-1624.

[29] N.R. Council, D.o. Earth, L. Studies, R.S. Board, C.o.W.F. Technology, Waste forms technology and performance, National Academies Press, 2011.

[30] H. Boucetta, R. Podor, L. Stievano, J. Ravaux, X. Carrier, S. Casale, S.p. Gossé, A.l. Monteiro, S. Schuller, Mechanism of RuO_2 crystallization in borosilicate glass: an original in situ ESEM approach, Inorganic Chemistry, 51 (2012) 3478-3489.

[31] J.A. Rodriguez, J.C. Hanson, A.I. Frenkel, J.Y. Kim, M. Pérez, Experimental and theoretical studies on the reaction of H_2 with NiO: role of O vacancies and mechanism for oxide reduction, Journal of the American Chemical Society, 124 (2002) 346-354.

[32] W.E. Bell, M. Tagami, High-temperature chemistry of the Ruthenium—Oxygen system, The Journal of Physical Chemistry, 67 (1963) 2432-2436.

[33] Y. Okamoto, H. Shiwaku, M. Nakada, S. Komamine, E. Ochi, M. Akabori, REDOX state analysis of platinoid elements in simulated high-level radioactive waste glass by synchrotron radiation based EXAFS, Journal of Nuclear Materials, 471 (2016) 110-115.

[34] S. Biswas, J. Mukerji, Solubility of ruthenium in silicate and phosphate glasses, Cent. Glass Ceram. Res. Inst. Bull., 15 (1968) 99-103.

[35] J. Mukerji, S. Biswas, Solubility of ruthenium in soda silica glasses, Cent. Glass Ceram. Res. Inst. Bull., 14 (1967) 30-34.

[36] I.M. Lifshitz, V.V. Slyozov, The kinetics of precipitation from supersaturated solid solutions, Journal of Physics and Chemistry of Solids, 19 (1961) 35-50.

[37] C.T. Campbell, Ultrathin metal films and particles on oxide surfaces: structural, electronic and chemisorptive properties, Surface Science Reports, 27 (1997) 1-111.

[38] W. Ostwald, On the assumed isomerism of red and yellow mercury oxide and the surface-tension of solid bodies, Z. Phys. Chem, 34 (1900) 495-503.

[39] A. Simo, J.r. Polte, N. Pfander, U. Vainio, F. Emmerling, K. Rademann, Formation mechanism of silver nanoparticles stabilized in glassy matrices, Journal of the American Chemical Society, 134 (2012) 18824-18833.

[40] Z. Zhang, Z. Wang, S. He, C. Wang, M. Jin, Y. Yin, Redox reaction induced Ostwald ripening for size-and shape-focusing of palladium nanocrystals, Chemical Science, 6 (2015) 5197-5203.

Figure Captions

Fig. 1 FESEM images of glass samples with different RuO_2 contents: (a) Ru0.01, (b) Ru0.02, (c) Ru0.04, and (d) Ru0.1.

Fig. 2 XRD patterns of glass samples with different RuO_2 contents heat-treated at 1200 °C for 30, 60, 120, and 180 min. Al_2O_3 was added as the internal standard for quantitative analysis.

Fig. 3 Back-scattered SEM images showing the morphology of RuO_2 and the distribution of metallic Ru^0 n in the Ru4.0 glass sample.

Fig. 4 Rietveld refinement of the XRD patterns of glass samples for semiquantitative phase analysis of crystalline RuO_2 and metallic Ru^0: (a) Relationships between the contents of RuO_2 crystals and metallic Ru^0 precipitated from the glass melt and the added RuO_2 content; (b) volatilization and precipitation of Ru as a function of the added RuO_2 content.

Fig. 5 SEM images of RuO_2 crystals and their size distributions: (a and d) PR, (b and e) PR30, (c and f) Ru0.5, (g and j) Ru1.0, (h and k) Ru4.0, and (i and l) Ru6.0.

Fig. 6 FESEM images showing the morphology of RuO_2 crystals precipitated in Ru0.5 glass with different melting temperatures and durations.

Fig. 7 3D diagram correlating the heat-treatment temperatures, durations, and average crystal sizes.

Fig. 8 Size distributions of RuO_2 crystals in glass for 5, 50, 180, and 300 min at (a-d) 1200 °C and (e-h) 1300 °C.

Fig. 9 Time evolution of the RuO_2 crystal size at 1200 °C and 1300 °C and linear fits for the Ru0.5 glass.

Fig. 10 Schematic diagram of the formation mechanism of polyhedral RuO_2 crystals.

Table 1 Composition of simplified nuclear waste glass (wt.%)

Oxide	Nominal composition	Measured composition
SiO_2	50	49.70
B_2O_3	18.89	18.51
Al_2O_3	6.67	8.85
Li_2O	2.78	2.77
Na_2O	13.33	12.54
CaO	5.00	4.76
ZrO_2	3.33	2.87
Sum	100.00	100.00

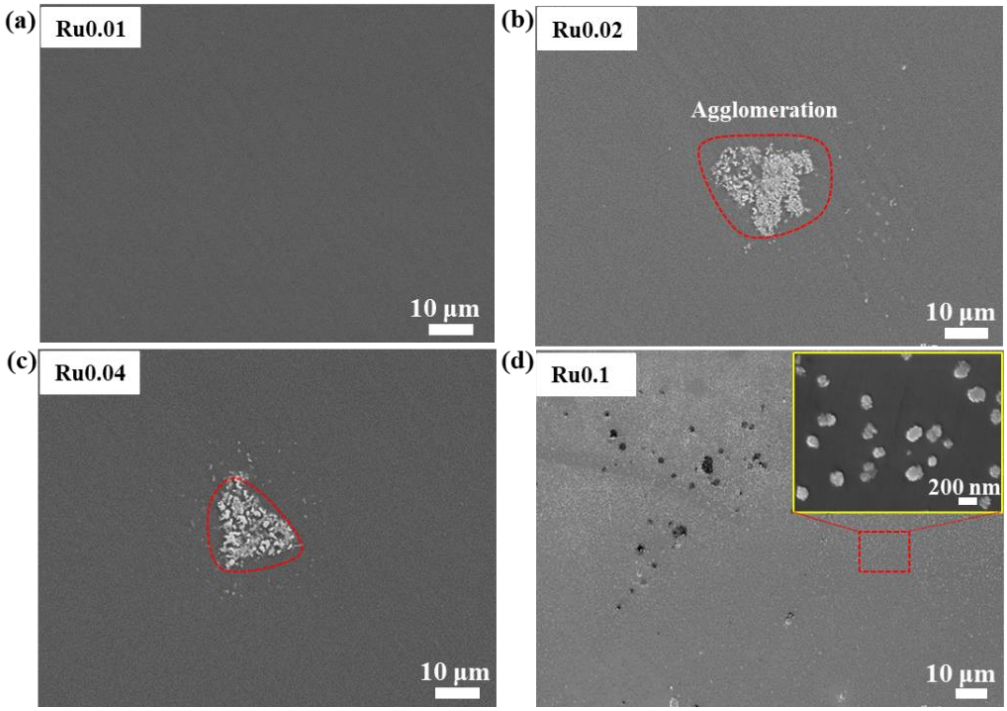
(a)
Ru0.01
10 µm
(b)
Ru0.02
Agglomeration
10 µm
(c)
Ru0.04
10 µm
(d)
Ru0.1
200 nm
10 µm

Fig. 1

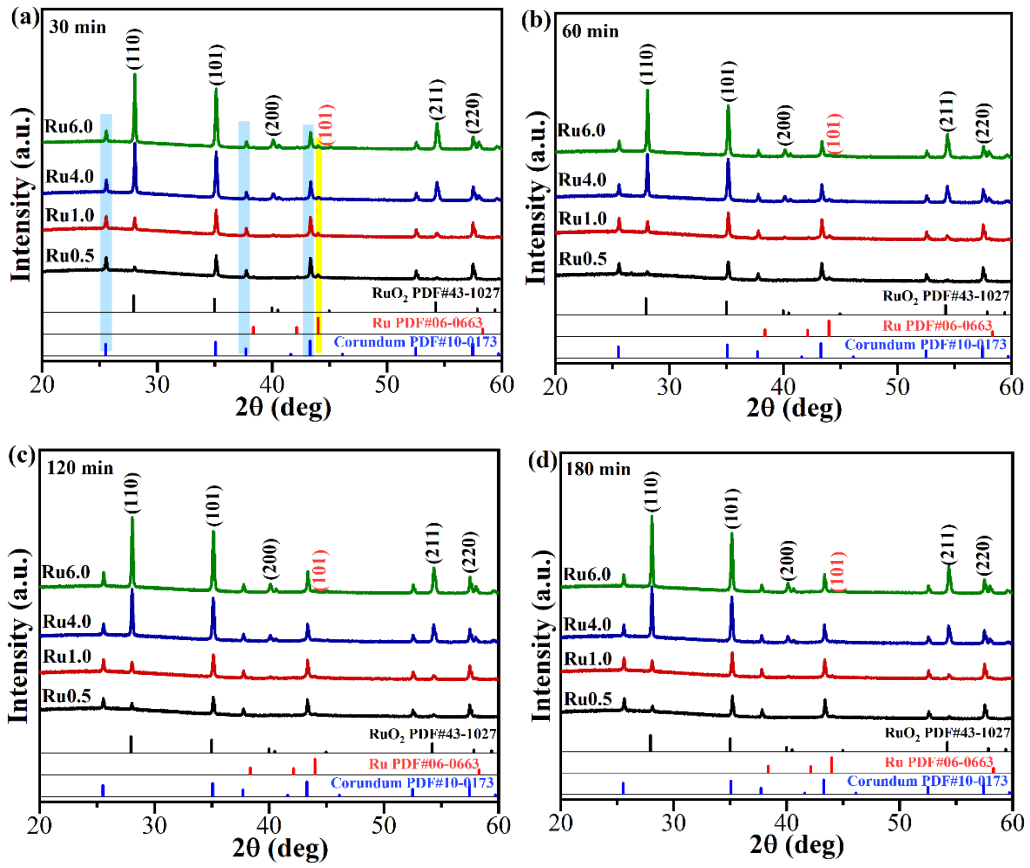
(a)
30 min
(b)
60 min
(c)
120 min
(d)
180 min
Intensity (a.u.)
2θ (deg)
Ru6.0
Ru4.0
Ru1.0
Ru0.5
(110)
(101)
(200)
(101)
(211)
(220)
RuO2 PDF#43-1027
Ru PDF#06-0663
Corundum PDF#10-0173

Fig. 2

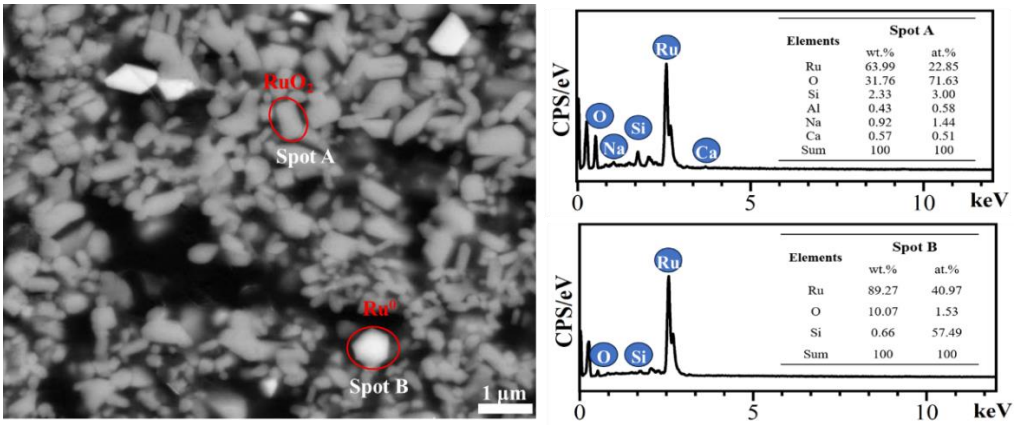
RuO2
Spot A
Ru0
Spot B
1 µm
CPS/eV
Ru
O
Si
Na
Ca
0
5
10
keV
Elements
Spot A
wt.%
at.%
Ru 63.99 22.85
O 31.76 71.63
Si 2.33 3.00
Al 0.43 0.58
Na 0.92 1.44
Ca 0.57 0.51
Sum 100 100
CPS/eV
Ru
O
Si
0
5
10
keV
Elements
Spot B
wt.%
at.%
Ru 89.27 40.97
O 10.07 1.53
Si 0.66 57.49
Sum 100 100

Fig. 3

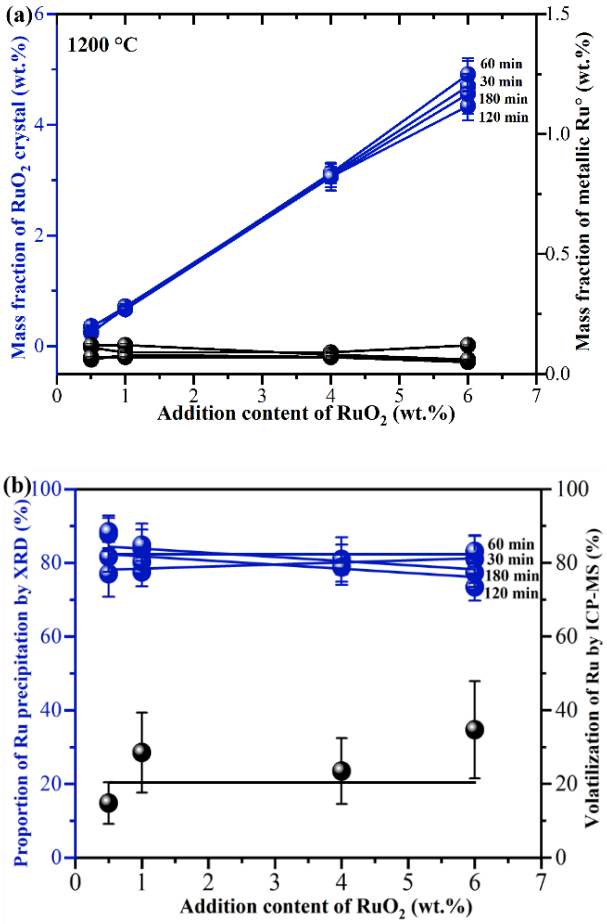
(a)
1200 °C
60 min
30 min
180 min
120 min
Mass fraction of RuO2 crystal (wt.%)
Mass fraction of metallic Ru° (wt.%)
Addition content of RuO2 (wt.%)
(b)
60 min
30 min
180 min
120 min
Proportion of Ru precipitation by XRD (%)
Volatilization of Ru by ICP-MS (%)
Addition content of RuO2 (wt.%)

Fig. 4

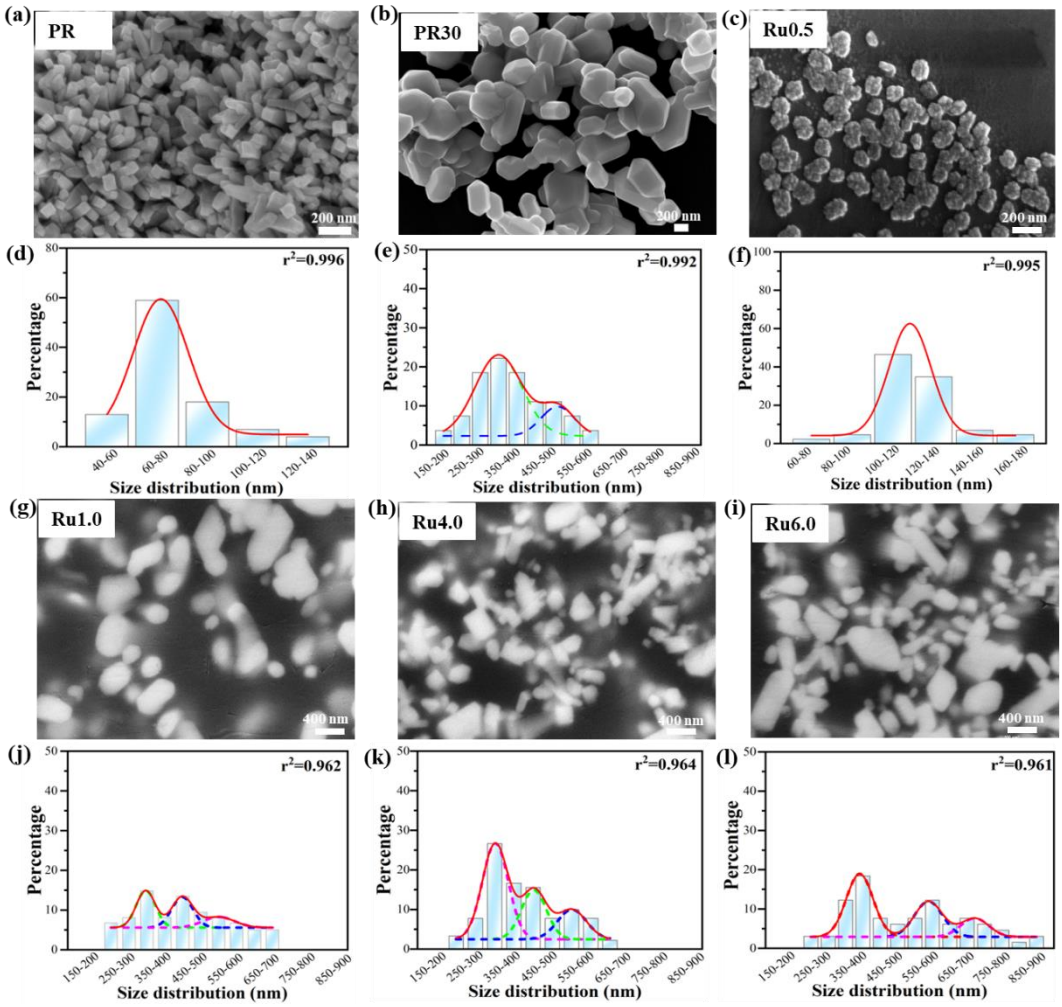
(a)
PR
200 nm
(b)
PR30
200 nm
(c)
Ru0.5
200 nm
(d)
r²=0.996
Percentage
Size distribution (nm)
(e)
r²=0.992
Percentage
Size distribution (nm)
(f)
r²=0.995
Percentage
Size distribution (nm)
(g)
Ru1.0
400 nm
(h)
Ru4.0
400 nm
(i)
Ru6.0
400 nm
(j)
r²=0.962
Percentage
Size distribution (nm)
(k)
r²=0.964
Percentage
Size distribution (nm)
(l)
r²=0.961
Percentage
Size distribution (nm)

Fig. 5

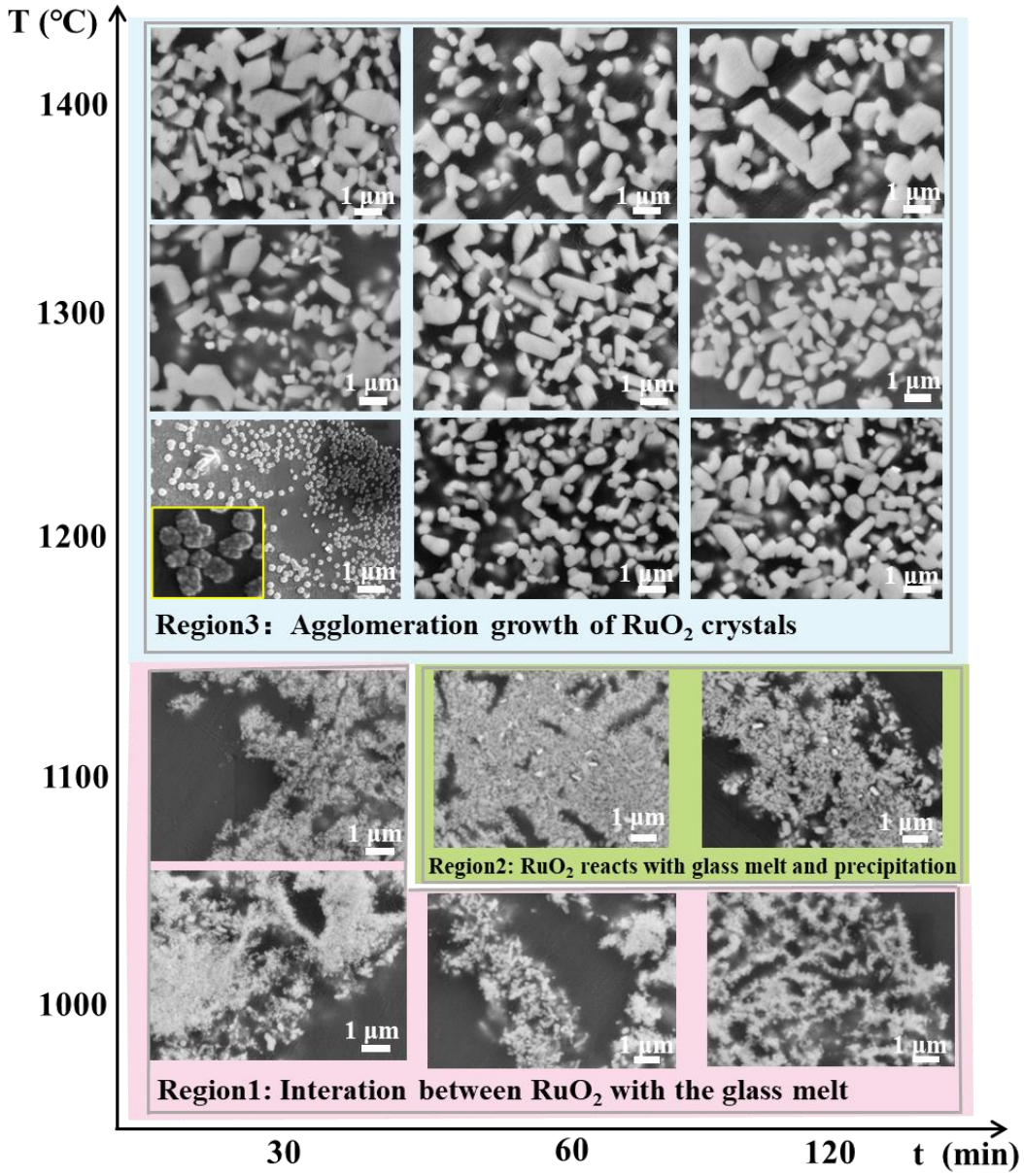
T (°C)
1400
1300
1200
1100
1000
1 μm
Region3： Agglomeration growth of RuO_2 crystals
Region2: RuO_2 reacts with glass melt and precipitation
Region1: Interation between RuO_2 with the glass melt
30
60
120
t (min)

Fig. 6

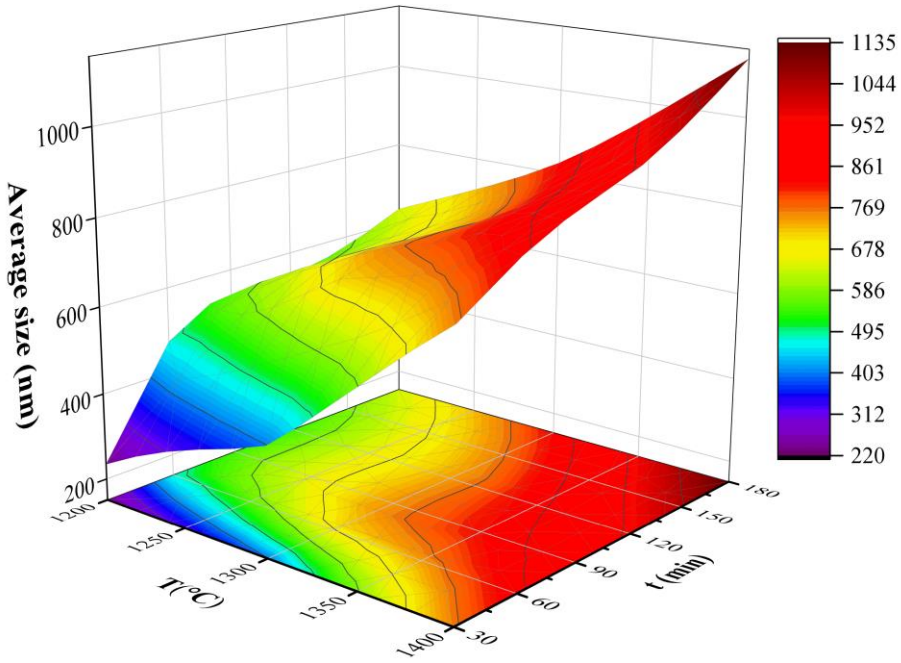
Average size (nm)
1000
800
600
400
200
1200
1250
1300
1350
1400
T(°C)
30
60
90
120
150
180
t (min)
1135
1044
952
861
769
678
586
495
403
312
220

Fig. 7

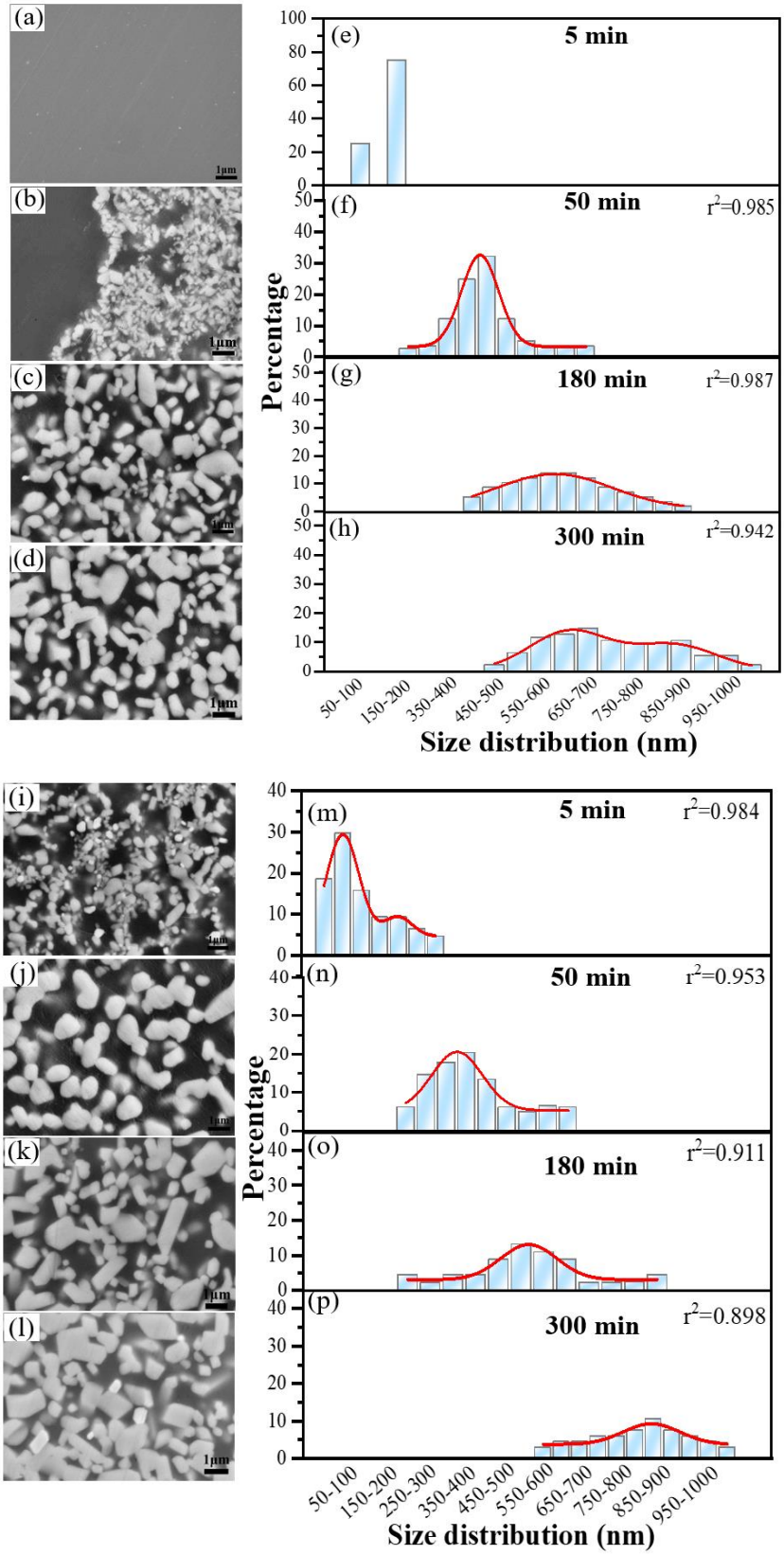
(a)
(b)
(c)
(d)
(e) 5 min
(f) 50 min r²=0.985
(g) 180 min r²=0.987
(h) 300 min r²=0.942
Percentage
50-100
150-200
350-400
450-500
550-600
650-700
750-800
850-900
950-1000
Size distribution (nm)
(i)
(j)
(k)
(l)
(m) 5 min r²=0.984
(n) 50 min r²=0.953
(o) 180 min r²=0.911
(p) 300 min r²=0.898
Percentage
50-100
150-200
250-300
350-400
450-500
550-600
650-700
750-800
850-900
950-1000
Size distribution (nm)

Fig. 8

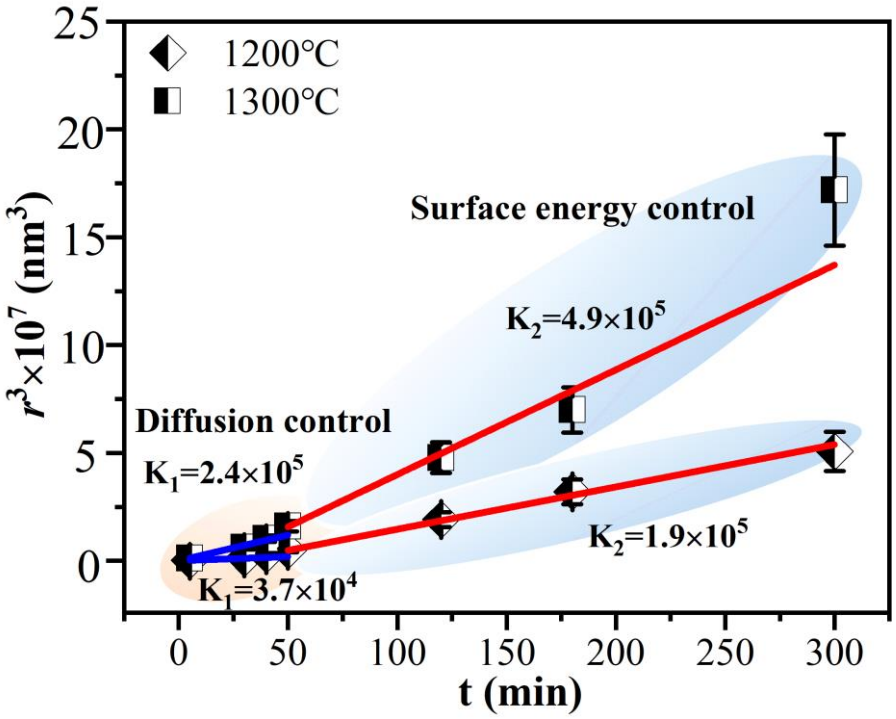
1200°C
1300°C
Surface energy control
K_2=4.9×10^5
Diffusion control
K_1=2.4×10^5
K_2=1.9×10^5
K_1=3.7×10^4
r^3×10^7 (nm^3)
t (min)
0
5
10
15
20
25
0
50
100
150
200
250
300

Fig. 9

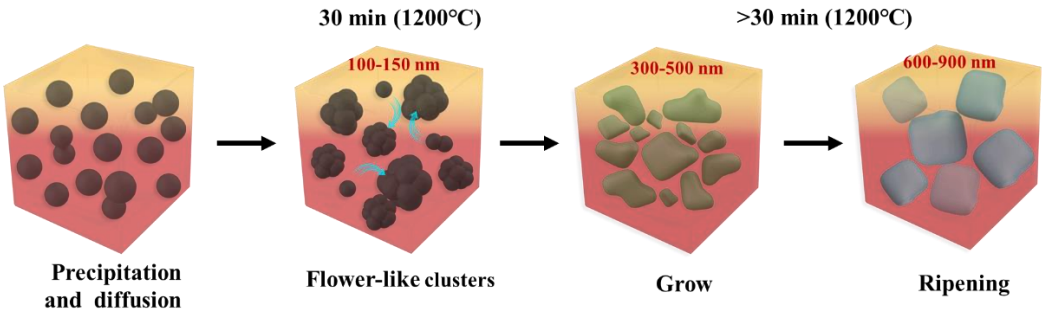
30 min (1200°C)
>30 min (1200°C)
100-150 nm
300-500 nm
600-900 nm
Precipitation and diffusion
Flower-like clusters
Grow
Ripening

Fig. 10